ELSEVIER

Journal of Nuclear Materials 266–269 (1999) 1028–1033

journal of nuclear materials

Behaviour of upstream separatrix density in JET H-mode plasmas

S.J. Davies [a,*], S.K. Erents [b,1], P.C. Stangeby [c], J. Lingertat [a], G.F. Matthews [a], R.D. Monk [a], G.C. Vlases [a]

[a] JET Joint Undertaking, Abingdon, Oxon, OX14 3EA, UK
[b] UKAEA Fusion, Culham (UKAEA/Euratom Fusion Association), Abingdon, Oxon, OX14 3DB, UK
[c] University of Toronto, Institute for Aerospace Studies, Toronto, Canada M3H 5T6

Abstract

The variation of $n_e^{Sep}/\overline{n}_e$ in JET H-modes is described. The upstream separatrix density, n_e^{Sep}, was determined using total pressure balance, in conjunction with 'onion-skin' modelling and reciprocating Langmuir probe measurements. It was found that the ratio $n_e^{Sep}/\overline{n}_e$ was strongly influenced by ELM frequency increasing, proportional to the rate of particle loss to the scrape-off layer (SOL) from ELMs, towards the pedestal density and then saturating. The initial $n_e^{Sep}/\overline{n}_e$ ratio and rate of increase were different for horizontal and vertical target configurations with the latter having an initial $n_e^{Sep}/\overline{n}_e$ ratio of 0.12. Related information on the behaviour of the density SOL width and the variation of $n_e^{Sep}/\overline{n}_e$ with confinement are also presented.

Keywords: ELMyH-mode; Density increase; JET; Separatrix

1. Introduction

Information on the behaviour of the upstream separatrix density, n_e^{Sep}, is important because it strongly influences conditions at the divertor target. For example, with 9–10 MW of power into the scrape-off layer (SOL), it was found that $n_e^{tgt} \propto (n_e^{Sep})^{1.6}$ under high recycling or conduction limited regimes. It has also been postulated that n_e^{Sep} may play a role in the loss of confinement in H-modes [1,2]. To allow comparison with other tokamaks and to the required ITER conditions the ratio $n_e^{Sep}/\overline{n}_e$ is presented. In L-mode a $n_e^{Sep}/\overline{n}_e$ ratio of approximately one-third is generally assumed as reported elsewhere [3–5]. In H-mode the situation is further complicated by the formation of the pedestal and the presence of ELMs. There is also the difficulty in locating with sufficient accuracy the separatrix position owing to the smaller SOL width. The present ITER design considers a fixed $n_e^{Sep}/\overline{n}_e$ consistent with the reported findings for L-mode which is found not to be the case for JET H-mode plasmas.

The variation in n_e^{Sep} between ELMs for fuelling scans in horizontal and vertical target configurations using the JET MkIIA and MkIIAP divertor is presented here. Following this introduction a description of the method for determining the separatrix position using total pressure balance is given. The behaviour of the separatrix density, which was found to be strongly influenced by ELM frequency and different for horizontal and vertical target configurations, is then given. Note that separatrix values given here are for between ELMs at the outer midplane. Finally, related information on the behaviour of the density SOL width and the variation of $n_e^{Sep}/\overline{n}_e$ with confinement are presented.

2. Determination of upstream separatrix position

The determination of the upstream separatrix from magnetic equilibrium reconstruction is difficult because

* Corresponding author. Tel.: +44 1235 465282; fax: +44 1235 464766; e-mail: sdavies@jet.uk

[1] Jointly funded by the UK Department of Trade and Industry and Euratom.

0022-3115/99/$ – see front matter
PII: S0022-3115(98)00683-7

it has an uncertainty of 1 cm which is comparable to the SOL width. The approach taken at JET is to use total pressure balance, in conjunction with 'onion-skin' modelling (OSM) [6] and upstream reciprocating Langmuir probe measurements, in the following manner:

1. Separatrix at target defined as peak in T_e^{Tgt} and/or J_{sat}^{Tgt}.
2. $T_i^{Tgt} = T_e^{Tgt}$ assumed, consistent with equipartition criteria [7].
3. Upstream total pressure calculated using OSM n_e^{Up}, T_e^{Up} and T_i^{Up} and found to be

$$n_e^{Up}(T_i^{Up} + T_e^{Up}) \approx 2n_e^{Tgt}(T_i^{Tgt} + T_e^{Tgt}) = 4n_e^{Tgt}T_e^{Tgt} \quad (1)$$

4. Reciprocating probe total pressure profile, calculated using measured T_e^{Up} and OSM T_i^{Up}/T_e^{Up} ratio, shifted to match OSM.

OSM has its boundary conditions specified at the target from Langmuir probe measurements which give the initial 2D variation, Fig. 1. The conservation equations are solved in 1D along each flux tube using NIMBUS, which is a neutral hydrogenic Monte Carlo code [8], to provide the hydrogenic ionisation and power terms. Within the OSM it is possible to adjust the T_i^{Tgt}/T_e^{Tgt} ratio to account in some way for the poor power balance observed in these H-modes as observed elsewhere [9]. The target probes calculated at most 1.5 MW to the target (using $T_i^{Tgt} = T_e^{Tgt}$) with approximately 6 MW expected from global parameters. Adjusting T_i^{Tgt} to obtain power balance required T_i^{Tgt}/T_e^{Tgt} ratios of up to 20 and was inconsistent with equipartition [7]. Using $T_i^{Tgt}/T_e^{Tgt} > 1$ would increase the $n_e^{Sep}/\overline{n}_e$ ratios presented here by ~0.1.

An example of the upstream total pressure profile obtained from the OSM and reciprocating probe data is shown in Fig. 2(a). The scatter in the experimental data arises from fluctuations [10] and because the reciprocating probe could not, in this instance, distinguish between individual ELMs. Other measurements using a triple Langmuir probe array were able to distinguish between individual ELMs. The corresponding upstream density profiles are shown in Fig. 2(b). Note the steeper gradient of the pressure profile within 5 mm of the separatrix which then broadens to become comparable to the density scrape-off width. This is a consequence of the temperature profile, which has a steep gradient up to 5 mm from the separatrix and then flattens, whilst the density profile is observed to have a constant scrape-off width.

Reciprocating probe measurements can also be used to determine separatrix densities for detached divertor conditions where the OSM is invalid. Analysis of attached cases gives the absolute position of the separatrix, assuming this does not change for the same magnetic equilibrium during detachment, the location of the reciprocating probe measurement relative to this can be determined, and if required, its profile extrapolated to the separatrix.

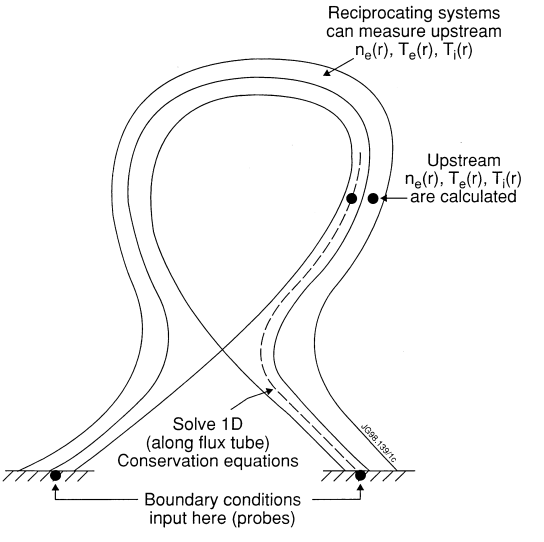

Fig. 1. Schematic of 'onion-skin' layers in SOL modelling.

3. General behaviour and conditions at target during H-mode fuelling scan

Separatrix densities between ELMs at the outer midplane were determined for a series of H-mode fuelling scans performed:

1. at fixed field and current (2.3 T/2.3 MA, 2.5 T/2.5 MA and 3 T/3 MA),
2. with 12 MW NBI heating,
3. with unplugged (MkIIA) and plugged (MkIIAP) divertor,
4. on horizontal (H/SFE) and vertical (V/SFE) target,
5. with low (LT) and high (HT) triangularity (LT have $\Delta \leqslant 0.2$, HT have $\Delta \geqslant 0.3$).

With increasing D_2-fuelling rate, $\overline{n}_e$ and the confinement factor, H97, reach a limit and then decrease with further fuelling whilst the ELM frequency continues to increase [11]. The H/SFE/LT configuration attains a peak $\overline{n}_e$ of typically 7.3×10^{19} m^{-3} which is 78% of the Greenwald density limit for both MkIIA and MkIIAP whilst its HT equivalent attains a peak $\overline{n}_e$ of typically 9.1×10^{19} m^{-3}, 94% of the Greenwald density limit. In comparison the V/SFE/LT configuration attains a peak $\overline{n}_e$ of typically 7.6×10^{19}m^{-3}, 77% of the Greenwald density limit, and a peak $\overline{n}_e$ of typically 8.3×10^{19} m^{-3}, 80% of the Greenwald density limit, for the HT case.

Comparison of the horizontal/vertical target parameters given in Table 1 shows a higher electron temperature for the inner horizontal target than for the vertical, with comparable ion-flux, whilst on the outer

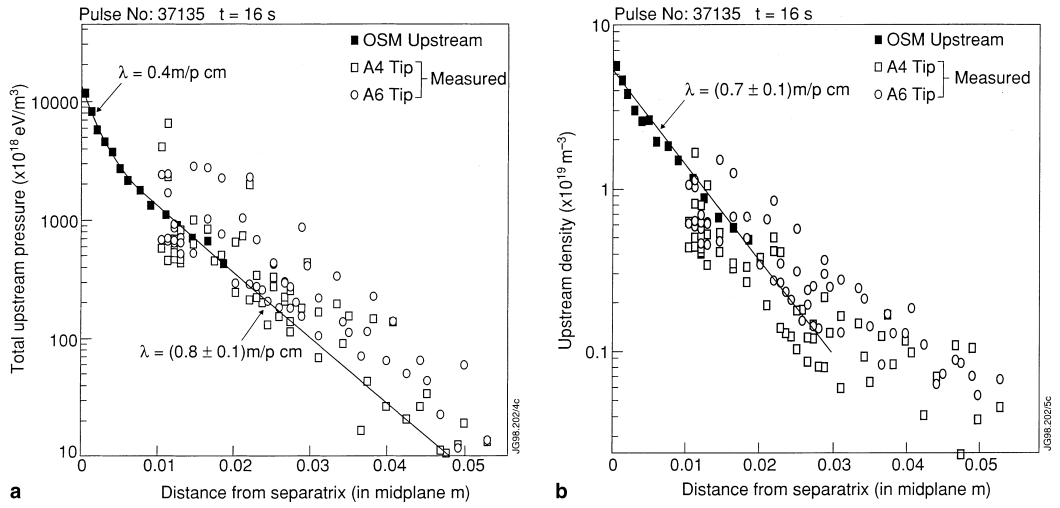

Fig. 2. (a) OSM calculated and reciprocating probe derived upstream total pressure profiles, and (b) corresponding upstream density profiles. λs are given in midplane cm (m/p cm).

target, the electron temperature decreases at a lower rate for the horizontal target which also has a higher ion-flux. The equivalent unplugged MkIIA sequence of Table 1 had decreased inner and outer electron temperatures (up to a factor of 2) with similar inner ion-fluxes and lower outer ion-fluxes. The main differences with H/SFE/HT configurations are lower inner ion-flux (up to factor of 2) and slightly lower outer electron temperature, with similar changes to LT in going from MkIIa to MkIIAP except for the outer ion-flux which is up to 1.5× higher in MkIIa. Main differences for the V/SFE/HT configuration are an initially higher outer electron temperature for MkIIA which then decreases at higher fuelling rates as for LT, Table 1, and converges to the MkIIAP values. The outer ion-flux is also higher for MkIIA/V/SFE/HT.

4. Behaviour of n_e^{Sep} with ELM frequency

It was found that n_e^{Sep} varied most strongly with ELM frequency, Fig. 3, and because of the relation between ELM frequency and triangularity [12], for the same target configuration a difference in the rate of increase in $n_e^{Sep}/\overline{n}_e$ is observed for LT and HT. No difference exists between the unplugged (MkIIA) and plugged (MkIIAP) divertor, for the same configuration and triangularity. The only major change that was observed in going from MkIIa to MkIIAP was a ~35% decrease in the midplane pressure [1] with no significant change in confinement, $\overline{n}_e$ or divertor pressure. Fig. 3(b) also shows that the vertical target has both a lower $n_e^{Ped}/\overline{n}_e$ and $n_e^{Sep}/\overline{n}_e$ ratio. The lowest $n_e^{Sep}/\overline{n}_e$ ratio is 0.12 for the V/SFE/HT configuration.

Table 1
Comparison of target parameters between horizontal and vertical target configurations

Fuelling rate (×10^{22} elec/s)	Inner			Outer		
	Peak Te (eV)	Peak ion-flux (A/cm^2)	Integrated ion-flux (×10^{22}/s)	Peak Te (eV)	Peak ion-flux (A/cm^2)	Integrated ion-flux (×10^{22}/s)
Horizontal target configuration: MkIIAP/H/SFE/LT						
0	20	21.0	3.8	30	23.7	3.2
1.4	16	36.8	6.7	35	64.3	9.0
2.2	9	34.7	6.4	21	83.1	14.0
2.8	8	38.0	3.2	19	77.6	9.7
Vertical target configuration: MkIIAP/V/SFE/LT						
0	7.5	7.0	2.6	30.7	8.7	3.8
1.4	7	39.9	7.4	15.1	22.7	5.0
2.1	6	26.2	4.5	10	24.7	4.1
2.8	5	45.3	7.5	6	27.3	6.3
3.5	6	24.6	4.0	6	29.2	6.7

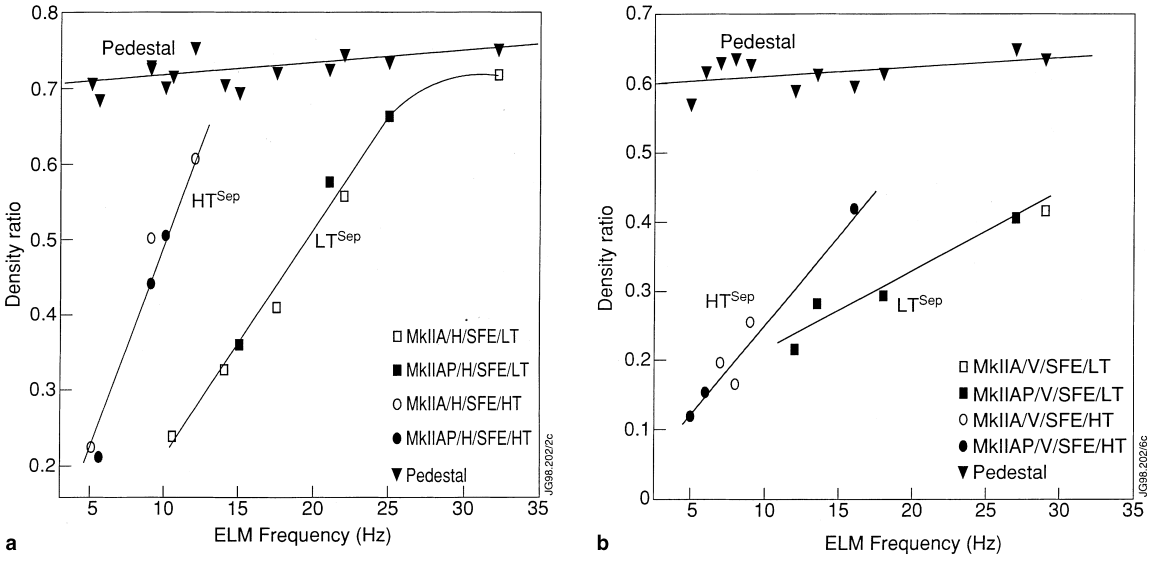

Fig. 3. Variation of $n_e^{Sep}/\bar{n}_e$ as a function of ELM frequency for (a) horizontal target and (b) vertical target configurations.

For all cases, n_e^{Sep} is seen to increase towards the pedestal density and saturate at a rate dependent on triangularity and target configuration. This results in $n_e^{Sep}/\bar{n}_e$ ratios of up to 0.72, Fig. 3(a), which has also been found on DIIID [13] and ASDEX-U [14]. In addition the DIIID results had $n_e^{Sep}/\bar{n}_e$ ratios as low as 0.15 and found that it increased with upstream electron pressure, speculating that this dependence is related to ELM activity. If the two-point model [15] were used to calculate the upstream parameters then the $n_e^{Sep}/\bar{n}_e$ ratios quoted here would be reduced by up to a factor of 2. The main difference of the more refined OSM from the two-point model is the inclusion of parallel ion heat convection and radiation in the edge. Consistent with most modelling, it calculates n_e^{Sep} accurate to within a factor of 2. Whilst the reciprocating probe measurements verify the OSM calculations, the scatter in the data in these ELMy H-modes is often of the same magnitude. As mentioned before, determination of the separatrix from magnetic equilibrium reconstruction is not sufficiently accurate in H-modes and would lead to even higher errors in n_e^{Sep}. The fact that n_e^{Sep} values presented here do not exceed the pedestal values gives some confidence in the data and perhaps represents its upper limit. It is important to emphasise, however, that it does not alter the trends described here and shown in Figs. 3 and 4.

The correlation of n_e^{Sep} with ELM frequency, f_{ELM}, shown in Fig. 3 led to the hypothesis that the increase in n_e^{Sep} was proportional to rate of particle loss to the SOL from ELMs, i.e. $\propto f_{ELM}*\Delta n_e^{Edge}$. Generally the characteristics of LT pulses are high f_{ELM} with a lower drop in edge pedestal density per ELM, Δn_e^{Edge}, whilst HT pulses are characterised by low f_{ELM} and higher Δn_e^{Edge}. Fig. 4 illustrates the increase in n_e^{Sep} as a function of $f_{ELM}*\Delta n_e^{Edge}$ which, for a given target configuration, unites both the LT and HT data in support of this hypothesis. The difference in target configuration remains, however, which is reflected by the difference in target parameters,Table 1.

The saturated n_e^{Sep} for H/SFE data at $f_{ELM}*\Delta n_e^{Edge} > 550 \times 10^{18}$ m^{-2}/s were obtained from reciprocating measurements only, using the method described in Section 2, as detachment at the target had

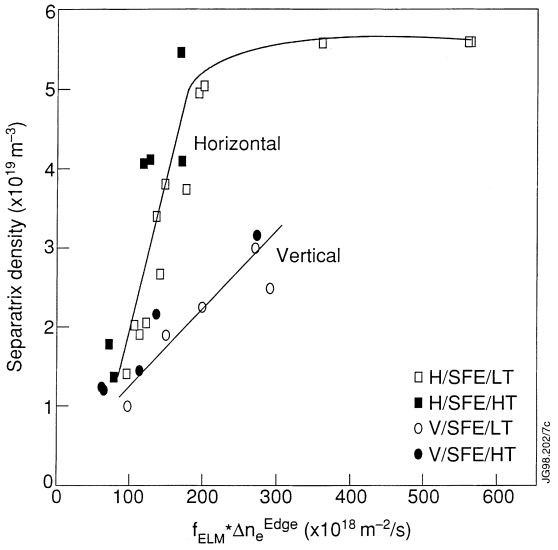

Fig. 4. Variation in n_e^{Sep} for horizontal and vertical target configurations as a function of particle loss to SOL.

occurred at these higher ($\Phi > 2.8 \times 10^{22}$ elec/s) fuelling rates. Comparable data for V/SFE were not available as the vertical target more readily detaches, Table 1, and because there were no reciprocating measurements in these pulses.

5. Behaviour of SOL width

As well as a variation in n_e^{Sep}, changes to the density SOL width were observed. The between ELMs, density SOL width mapped in flux space to the outer midplane, λ_{ne}, was found to be slightly smaller for the vertical target configuration with LT ($\lambda_{ne} = 0.3$ midplane cm for MkIIAP/V/SFE/LT with no fuelling) than for the equivalent horizontal case ($\lambda_{ne} = 0.44$ midplane cm) in these H-mode pulses. Typical flux expansions from the target and from the reciprocating system to the outer midplane were $\geqslant 10$ and ~ 2.5 respectively so that these small values could be resolved from the data.

With HT no significant difference was found between the horizontal and vertical target, Fig. 5. Code simulations [16] predict a thinner SOL width for a vertical target as a result of differences in the recycling pattern which has been observed in L-mode [17] with $\lambda_{ne}^{Vert} \approx 1/2\lambda_{ne}^{Horz}$ although this is not a direct one-to-one comparison as they were at different stages of detachment. These data show that the difference is not so large in H-mode under more comparable main plasma conditions. A broadening of the SOL width as the target conditions approach detachment does occur, consistent with previous observations [18], with $\lambda_{ne} = 0.55$ midplane cm for MkIIAP/H/SFE/LT at a fuelling rate, Φ, of 2.2×10^{22} elec/s.

No difference was seen, Fig. 5, for both LT and HT in the upstream profiles for the horizontal target between unplugged (MkIIA) and plugged (MkIIAP). In contrast there was a significant decrease in the upstream density for the V/SFE/HT configuration in going from MkIIA to MkIIAP which is a consequence of the electron temperature and ion-flux being lower in the MkIIAP case as described in Section 3.

6. Variation with confinement factor, H97

The confinement factor, H97 (corrected for fast ions), has been found to be related to ELM frequency, f_{ELM}, by [19]

$$H97 = 1.23 - 0.57 f_{ELM}\tau\{1 - \exp[-1/(f_{ELM}\tau)]\} \quad (2)$$

where $\tau = 0.034$ s has been determined from the experimental data and is representative of the time taken for the confined plasma to re-heat the edge pedestal following an ELM. It has been postulated [1] that it is n_e^{Sep} rather than an increased main chamber neutral pressure which produces the confinement degradation observed in these H-modes, because confinement quality was better correlated with divertor neutral pressure and with n_e^{Sep} than with midplane neutral pressure. The hypothesis being that in steady-state the exhaust rate must be equal to the fuelling rate and n_e^{Sep}, which is strongly related to $n_e^{Tgt}(\propto (n_e^{Sep})^{1.6})$ and thus the exhaust rate, will adjust in such a way so as to achieve this balance.

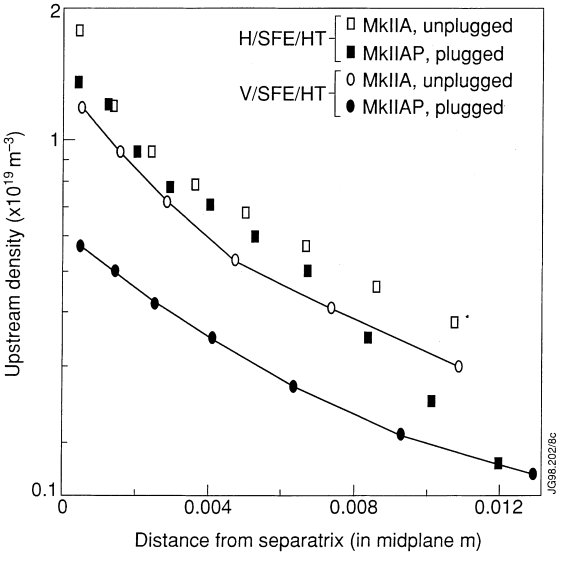

Fig. 5. Comparison of upstream density profiles for unplugged (MkIIA) and plugged (MkIIAP) divertor with no additional gas fuelling.

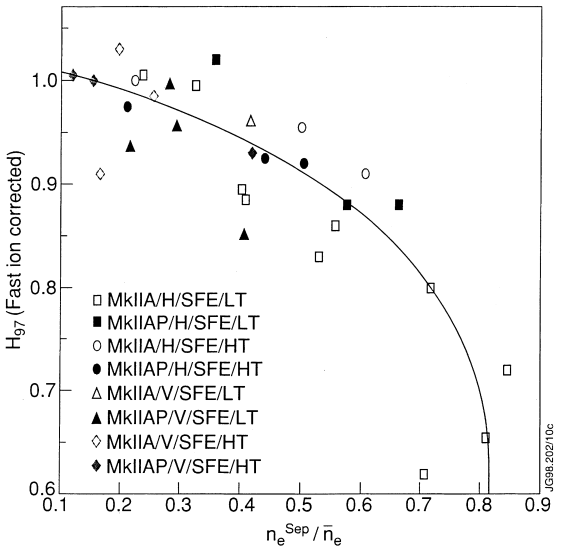

Fig. 6. Relation between confinement factor, H97, and $n_e^{Sep}/\bar{n}_e$ ratio. The line shown is for guidance of the variation only.

Fig. 6 shows how H97 (corrected for fast ions) varies with $n_e^{Sep}/\overline{n}_e$. The highest confinement is obtained for the smallest $n_e^{Sep}/\overline{n}_e$ and steadily decreases until n_e^{Sep} attains the pedestal value at H97 $\approx$ 0.8. As shown in Fig. 4, an increased exhaust rate results from increasing f_{ELM} brought about, in these H-modes, by increased gas fuelling. This is accompanied by an increase in n_e^{Sep} and consequent increase in n_e^{tgt} eventually leading to detachment which, recent modelling [20] would suggest, sets a limit on the maximum achievable n_e^{Sep}. Whether this then produces the observed loss of confinement or is just a reaction to the loss of confinement is still under investigation. Further comments on the density limit in H-modes can be found in [2].

7. Concluding remarks

Total pressure balance, in conjunction with OSM and upstream reciprocating probe measurements, has been used to determine n_e^{Sep} in H-mode plasmas over a variety of conditions. It was observed to increase towards the pedestal density $\propto f_{ELM}*\Delta n_e^{Edge}$ and saturate with the rate of increase being lower for the vertical target configuration. Whilst the value of n_e^{Sep} may be accurate up to within a factor of 2, consistent with most modelling and due to the scatter in the experimental measurements, it is important to emphasise that its behaviour with, for example, f_{ELM} remains the same.

The preferred ITER target configuration closest to these JET data is the V/SFE/HT which has $n_e^{Sep}/\overline{n_e}$ ratios ranging from 0.12 with $f_{ELM} = 5$ Hz to 0.45 for $f_{ELM} = 17$ Hz. A pragmatic approach to the calculation of f_{ELM} for ITER, based on observations from several tokamaks [21], gives a value of 1–2 Hz which, from these results, implies a low $n_e^{Sep}/\overline{n}_e$ ratio between ELMs making n_e^{Tgt} low and likely to be in the attached regime. Further studies to establish a suitable scaling to larger machine size of f_{ELM} are required, however, and there are other mechanisms, e.g. use of RF heating to produce smaller, more frequent ELMs, which could be used. Studies of how $n_e^{Sep}/\overline{n}_e$ scales between current tokamaks are also required, though the similarity between JET, DIIID [13] and ASDEX-U [14] results would suggest that it is invariant to machine size.

Further studies of JET data will include determination of n_e^{Sep} over a wider range of plasma current and toroidal field, to test the model of Ref. [20], and in lower density, higher f_{ELM}, RF heated H-mode fuelling scans.

References

[1] L.D. Horton et al., Studies in JET divertors of varied geometry I: non-seeded plasma operation, Nucl. Fusion, submitted.
[2] G.F. Matthews et al., these Proceedings.
[3] H. Murmann, M. Huang, Plas. Phys. Contr. Fus. 27 (1985) 103.
[4] K. McCormick et al., J. Nucl. Mater. 89 (1990) 176.
[5] D.N. Hill et al., J. Nucl. Mater. 204 (1992) 196.
[6] P.C. Stangeby, J.D. Elder, Nucl. Fusion 35 (1995) 1391.
[7] P.C. Stangeby, $T_i^{Tgt} > T_e^{Tgt}$ when $T_e^{Tgt} > [10^{-18}*L_c*n_e^{Tgt}*(T_i^{Tgt})^{0.5}]^{0.4}$, 1998, personal communication.
[8] E. Cupini et al., NET Report EUR MI 324/9, CEC Brussels, 1984.
[9] A. Loarte, PhD thesis, Universidad Complutense de Madrid 1992.
[10] I. Garcia-Cortes et al., Proceedings of the 24th EPS, Berchtesgaden, Germany, vol 21A, 1997, p. 109.
[11] G. Saibene et al., Proceedings of the 24th EPS, Berchtesgaden, Germany, vol 21A, 1997, p. 49.
[12] R. Mohanti et al., Proceedings of the 24th EPS, Berchtesgaden, Germany, vol 21A, 1997, p.101.
[13] R.A. Jong et al., J. Nucl. Mater. 800 (1992) 196.
[14] J. Schweinzer et al., these Proceedings.
[15] M. Keilhacker et al., Phys. Scr. T2/2 (1982) 443.
[16] A. Taroni et al., Contr. Plas. Phys. 32 (1992) 438.
[17] D.J. Campbell et al., in: Proceedings of the 15th International Conference on Plasma Physics Controlled Fusion, IAEA-CN-60/A-4I-4, 1994.
[18] G.F. Matthews et al., Plas. Phys. Contr. Fus. 37 (Suppl. 11A) (1995) A227.
[19] G. Fishpool, JET-P (97) 30 Nucl. Fusion, accepted.
[20] K. Borrass et al., Nucl. Fusion 37 (1997) 523.
[21] J. Lingertat et al., Proceedings of the Fourth Eur. Phys. Workshop, Stockholm, 1996.